Novel Optimal Load Control for Power System Frequency and Voltage Regulation

Yaxin Wang, Donglian Qi, Jianliang Zhang, and Jingcheng Mei

***Abstract*—The sudden generation-consumption imbalance is becoming more frequent in modern power systems, causing voltage and frequency stability issues. One potential solution is load participation in primary control. We formulate a novel optimal load control (NOLC) problem that aims to minimize the disutility of controllable loads in providing primary regulation. In this paper, we show that the network dynamics, coupled with well-defined load control (obtained via optimality condition), can be seen as an optimization algorithm to solve the dual problem of NOLC. Unlike most existing load control frameworks that only consider frequency response, our load-side primary control focuses on frequency, voltage, and aggregate cost. Simulation results imply that the NOLC approach can ensure better frequency and voltage regulations. Moreover, the coordination between NOLC and other devices enabled in the system, the NOLC performance against the total size of controllable loads, and the NOLC effectiveness in a multi-machine power system are also verified in MATLAB/Simulink.**

***Index Terms*—Novel optimal load control (NOLC), primary regulation, frequency response, voltage stability, smart load.**

I. Introduction

RECENTLY, large amounts of renewable energy generation and smart loads have been integrated into modern grids [1]. However, power imbalances are more likely due to intermittent renewable energy production and unpredictable electricity demand [2].

When the power supply or demand changes, the frequency and voltage deviate from the nominal values [3]. The control mechanisms are generally implemented on the generation side [4], [5] to maintain the frequency and voltage within acceptable ranges, which are referred to as primary, secondary, and tertiary controls, distinguished by their functions and timescales of operation [6].

Primary control is usually realized using traditional generators (TGs), which are completely decentralized and operate on a timescale of tens of seconds. It can rebalance the power and stabilize the frequency and voltage to new steady values. However, there are mechanical constraints on generator governors; thus, their regulating speeds are relatively slow. As the sudden generation-consumption imbalance becomes more frequent in modern power systems, conventional measures are incapable. Moreover, it is economically inefficient and environmentally unfriendly [7], [8].

Any action performed on the generation side (to guarantee a power balance between supply and demand) can also be implemented on the demand side [9]. Compared with traditional generators, smart switches on the user side offer controllable load opportunities to respond quickly [10]. Therefore, to relieve the pressure on generators, new technologies for power consumption control on the demand side are highly anticipated [11].

In the late 1970s, researchers introduced the concept of load participation in the primary control. Reference [12] studied the deployment of demand-side contribution as a provision or substitution of turbine-governed systems and spinning reserves. This point has been strengthened in the last decades with a large number of smart loads joining in the power systems [13]. The capability of a heat pump heater (HP) and battery to provide primary control was investigated in [14] without considering the customer comfort. Reference [15] utilized the potential of thermostatically controlled loads (TCLs) for frequency and voltage regulation through optimal management. Reference [16] showed that electric vehicles (EVs) are typical smart loads that can provide adequate reactive power on the residential side to compensate for power imbalances.

The aggregate disutility of consumers has not been considered in the literature mentioned above. Centralized optimization algorithms are more convenient for such a global optimization objective. However, they require complete communication and long computation time, especially in large-scale systems [17], [18]. Therefore, distributed algorithms have been developed [19].

Based on the perspective of network dynamics as distributed optimization algorithms, a "ubiquitous continuous fast-acting distributed primary frequency load control" called optimal load control (OLC) was first introduced in [20], which aims to minimize the aggregate disutility to utilities and consumers during the frequency regulation. They sought a systematic method to design the load-side primary frequency

Manuscript received: August 9, 2022; revised: November 22, 2022; accepted: January 10, 2023. Date of CrossCheck: January 10, 2023. Date of online publication: March 27, 2023.

This work was supported in part by the National Natural Science Foundation of China (No. U1909201).

This article is distributed under the terms of the Creative Commons Attribution 4.0 International License (http://creativecommons.org/licenses/by/4.0/).

Y. Wang, D. Qi (corresponding author), J. Zhang, and J. Mei are with the Electrical Engineering Department, Zhejiang University, Hangzhou, China, and D. Qi is also with the Hainan Institute of Zhejiang University, Sanya, China (e-mail: wangyaxin@zju. edu. cn; qidl@zju. edu. cn; jlzhang@zju. edu. cn; hzmeijc@zju.edu.cn).

DOI: 10.35833/MPCE.2022.000506

control for a pre-defined optimization problem. Moreover, the power consumption of each load can be controlled using local frequency measurements [21]. Subsequently, the application of OLC was investigated in [22], and the effects of choosing different disutility functions with respect to the frequency nadir and steady-state error were compared. The OLC theorem was further developed in [23], which considered the most suitable parameters for local load controllers via a multi-objective optimization procedure instead of using identical parameter settings. Similarly, considering the foundation of network dynamics as an optimization algorithm, [24] and [25] proposed a local volt/var control (LVC) for voltage regulation through the approach of reverse and forward engineering.

Although these primary response frameworks for smart loads involve only frequency control or voltage control, they present a new idea-network dynamics as optimization algorithms for the distributed control and optimization of modern power systems.

The intermittent power sources and time-varying load demands induce sudden power changes, resulting in frequency and voltage issues [26]. However, most existing methods focus on one or the other; for example, the traditional OLC [21] provided a primary frequency response while ignoring the potential of load participation in voltage regulation, or [25] and [27] proposed the distributed voltage control to cope with rapid voltage fluctuations introduced by renewable energy generation.

In this study, the novel optimal load control (NOLC) takes a step forward in the idea of network dynamics as optimization algorithms for power system frequency and voltage regulations. The NOLC approach has a universal applicability and fast response while accounting for aggregate disutility during load participation by inheriting the good properties of the traditional OLC. Distinguishing itself from the OLC, except for the generator dynamics, the variations in bus voltage and reactive power flow are also considered in the network dynamics. To support the primary regulation of both frequency and voltage, our contributions are focused on the following areas.

1) Complete network dynamics, which form the theoretical basis of load participation in primary frequency and voltage control simultaneously, are described.

2) An NOLC problem is formulated to minimize the aggregate disutility of rebalancing power by controllable loads.

3) We prove that the network dynamics can solve the dual NOLC problem obtained under the optimality condition. Thus, such optimality conditions develop a fundamental method for guiding the design of load control for the participation in primary regulation.

The rest of this paper is organized as follows. The model of network dynamics of the power system is described in Section II. The coupling of the network dynamics with the proposed NOLC is explained as a distributed optimization algorithm to address the dual problem of disutility minimization in Section III. The effect of NOLC on the system small-signal stability is investigated in Section IV. The simulation results are presented in Section V. The main conclusions and current limitations are discussed in Section VI.

II. Model of Network Dynamics

The power transmission network can be abstracted into a graph with (N,ε), where the vertex set N represents the buses in the power system; and edge set ε ($\varepsilon \subseteq N\times N$) represents the transmission lines in the power system. We assume that the graph is directed; therefore, if $e=(i,j)\in\varepsilon$, then $(j,i)\notin\varepsilon$. Other assumptions are listed as follows.

1) The lines $(i,j)\in\varepsilon$ are lossless and characterized by their reactance x_{ij}.

2) The voltage magnitudes of the generators are constant due to the strong excitation. However, the voltage magnitude variations on the other buses are considered.

3) The nominal phase angle difference is not ignored across each transmission line.

Under these assumptions, the subsequent network model distinguishes itself from the original model built in [20]-[23] by considering the variations in the bus voltage and reactive power flow. However, due to the ignorance of line resistance, both our analytical model and the models previously mentioned are more applicable to power systems with long-distance transmission.

A. Network Model

The complete network dynamics are described as preliminaries for the subsequent work. There are two types of buses: generator buses (G) and load buses (L) such that $G\bigcup L=N$. Among these, bus $j\in G$ has a generator that can convert the mechanical energy to electrical energy for the power supply, but bus $j\in L$ only has loads for power consumption. For further discussion, we divide the active loads into three types: frequency-sensitive, insensitive but controllable, and uncontrollable. Similarly, reactive loads can be classified as voltage-sensitive, insensitive but controllable, and uncontrollable ones.

1) Generator Buses

The swing equation of generator bus $j\in G$ can be written as:

$$H_j\Delta\dot{\omega}_j=P_j^{m'}-P_j^e-D_j'\Delta\omega_j \tag{1}$$

where H_j is the inertia constant of the generator; $\Delta\omega_j$ is the frequency deviation on bus j; $P_j^{m'}$ is the mechanical power of the generator; P_j^e is the electrical power; and D_j' is the damping coefficient.

Here, P_j^e includes not only the total active loads on bus j but also the net sum of branch active power flowing out and into bus j.

$$P_j^e=\hat{p}_j^0+D_j''\Delta\omega_j+p_j+p_j^l+\sum_{e\in\varepsilon}C_{je}P_e \tag{2}$$

where $\hat{p}_j^0$ is the nominal value of the frequency-sensitive active load on bus j; $D_j''\Delta\omega_j$ is the active power variation due to frequency deviation; p_j is the frequency-insensitive but controllable active load; p_j^l is the uncontrollable active load; C_{je} is the portion of the incidence matrix of the power transmission network [23]; and P_e is the branch power flow on

the transmission line $e=ij$ or $e=ji$, where i denotes the set of buses connected with j.

$$C_{je}=\begin{cases}1 & e=ji\in\varepsilon\\ -1 & e=ij\in\varepsilon\\ 0 & \text{otherwise}\end{cases} \tag{3}$$

We set P_j^m as an integrated active power injection equal to $P_j^{m'}-\hat{p}_j^0-p_j^l$ representing any active power injection from both the generation and load sides and $D_j=D_j'+D_j''$ for readability. The swing equation on the generator bus j can be rewritten as:

$$H_j\Delta\dot{\omega}_j=P_j^m-p_j-\sum_{e\in\varepsilon}C_{je}P_e-D_j\Delta\omega_j \tag{4}$$

Under the nominal operation, $P_j^{m,0}-p_j^0-\sum_{e\in\varepsilon}C_{je}P_e^0=0$. Hence, the deviation variables in (4) satisfy the following formula:

$$H_j\Delta\dot{\omega}_j=\Delta P_j^m-\Delta p_j-\sum_{e\in\varepsilon}C_{je}\Delta P_e-D_j\Delta\omega_j \tag{5}$$

In this study, the variations in the terminal voltage magnitude on the generator buses $j\in G$ are ignored. Therefore, $\left|V_j\right|_{j\in G}$ is assumed to be constant.

2) Load Buses

From (5), a load bus j with a small inertia can be expressed by an algebraic equation:

$$0=\Delta P_j^m-\Delta p_j-\sum_{e\in\varepsilon}C_{je}\Delta P_e-D_{jL}''\Delta\omega_j \tag{6}$$

where ΔP_j^m denotes the change in the integrated uncontrollable active loads. In addition, a load bus with high inertia can be treated as a generator bus [28].

The dynamics of voltage magnitude on bus $j\in L$ can be written as [29]:

$$K_j\Delta\dot{V}_j=-Q_j^e \tag{7}$$

where K_j is the coefficient related to voltage; ΔV_j is the voltage deviation on bus j; and Q_j^e is the reactive power imbalance on bus j.

$$Q_j^e=\hat{q}_j^0+D_{jL}\Delta V_j+q_j^l+q_j+\sum_{e\in\varepsilon}C_{je}Q_e \tag{8}$$

where $\hat{q}_j^0$ is the nominal value of the voltage-sensitive reactive load on bus j; $D_{jL}\Delta V_j$ is the reactive power variation due to voltage deviation; q_j is the voltage-insensitive but controllable reactive load; and q_j^l is the uncontrollable reactive load.

We set $Q_j^m=-\hat{q}_j^0-q_j^l$ as an aggregated uncontrollable reactive load. Hence, we have:

$$K_j\Delta\dot{V}_j=Q_j^m-D_{jL}\Delta V_j-q_j-\sum_{e\in\varepsilon}C_{je}Q_e \tag{9}$$

The deviation variables satisfy:

$$K_j\Delta\dot{V}_j=\Delta Q_j^m-D_{jL}\Delta V_j-\Delta q_j-\sum_{e\in\varepsilon}C_{je}\Delta Q_e \tag{10}$$

3) Power Flows

According to the power flow algebraic equation, the deviation of the active power branch flow (linearized) from bus i to bus j is:

$$\Delta P_{ij}=B_{ij}'\Delta V_i+B_{ij}''\Delta V_j+B_{ij}'''(\Delta\theta_i-\Delta\theta_j) \tag{11}$$

where $B_{ij}'=V_j^0\sin(\theta_i^0-\theta_j^0)/x_{ij}$, $B_{ij}''=V_i^0\sin(\theta_i^0-\theta_j^0)/x_{ij}$, and $B_{ij}'''=V_i^0V_j^0\cos(\theta_i^0-\theta_j^0)/x_{ij}$ are the constants determined from the nominal voltage magnitudes V_i^0 and V_j^0, phase angles θ_i^0 and θ_j^0, and line reactance, respectively.

Similarly, the deviation of the reactive power branch flow from bus i to bus j is represented as:

$$\Delta Q_{ij}=T_{ij}'\Delta V_i+T_{ij}''\Delta V_j+T_{ij}'''(\Delta\theta_i-\Delta\theta_j) \tag{12}$$

where $T_{ij}'=2V_i^0/x_{ij}-V_j^0\cos(\theta_i^0-\theta_j^0)/x_{ij}$; $T_{ij}''=-V_i^0\cos(\theta_i^0-\theta_j^0)/x_{ij}$; $T_{ij}'''=V_i^0V_j^0\sin(\theta_i^0-\theta_j^0)/x_{ij}$. The detailed derivation process is shown in Appendix A.

4) Network Model

For notational simplicity, the symbol Δ is omitted from the deviation variables. Therefore, a complete dynamic network model of the power system can be written as:

$$\dot{\theta}_j=\omega_j \tag{13}$$

$$H_j\dot{\omega}_j=P_j^m-p_j-\sum_{e\in\varepsilon}C_{je}P_e-D_j\omega_j\quad\forall j\in G \tag{14}$$

$$K_j\dot{V}_j=Q_j^m-D_{jL}V_j-q_j-\sum_{e\in\varepsilon}C_{je}Q_e\quad\forall j\in L \tag{15}$$

$$0=P_j^m-p_j-\sum_{e\in\varepsilon}C_{je}P_e-D_{jL}''\omega_j\quad\forall j\in L \tag{16}$$

$$P_{ij}=B_{ij}'V_i+B_{ij}''V_j+B_{ij}'''(\theta_i-\theta_j)\quad\forall(i,j)\in\varepsilon \tag{17}$$

$$Q_{ij}=T_{ij}'V_i+T_{ij}''V_j+T_{ij}'''(\theta_i-\theta_j)\quad\forall(i,j)\in\varepsilon \tag{18}$$

Note that all variables represent their deviations from the nominal values in the remainder of this paper.

III. NOLC

As a major shortening of load participation in primary control, most previous studies did not consider aggregate disutility from a global perspective in the controller design. We show that the network dynamics under optimality conditions adaptively solve the dual problem of a pre-defined disutility objective function. Therefore, such optimality condition develops a fundamental way to guide the design of local load control for participating in primary regulation, which is generally applicable to a class of the minimum disutility objectives that fits our assumption.

A. NOLC Problem

In this subsection, an NOLC problem is formulated to minimize the integrated negative effects on utilities and users while rebalancing the power to regulate both the system frequency and voltage. The objective function in the general form of (19a) indicates a class of optimization problems that represent the disutility caused by deviating from the normal power usage for the loads to participate in primary control. The optimization problem is subject to power balance constraints (19b).

$$\min_{\substack{\underline{p}_j\le p_j\le\bar{p}_j,\hat{p}_j,\\ \underline{q}_j\le q_j\le\bar{q}_j,\hat{q}_j}}\sum_{j\in N}\left\{c_{pj}(p_j)+c_{qj}(q_j)+\frac{\hat{p}_j^2}{2D_j}+\frac{\hat{q}_j^2}{2D_{jL}}\right\} \tag{19a}$$

s.t.

$$\begin{cases} p_j+\hat{p}_j=P_j^m-\sum_{e\in\varepsilon}C_{je}P_e \\ q_j+\hat{q}_j=Q_j^m-\sum_{e\in\varepsilon}C_{je}Q_e \end{cases} \tag{19b}$$

where $-\infty<\underline{p}_j\le\bar{p}_j<\infty$; and $-\infty<\underline{q}_j\le\bar{q}_j<\infty$.

The framework of the minimum disutility problem in (19a) consists of four parts. The first two parts $c_{pj}(p_j)$ and $c_{qj}(q_j)$ are the cost functions related to active or reactive controllable load power at bus j, respectively. The remaining two parts are assumed as the fixed items $\hat{p}_j^2/(2D_j)$ and $\hat{q}_j^2/(2D_{jL})$, which refer to the costs to frequency-sensitive load $\hat{p}_j:=D_j\omega_j$ and voltage-sensitive load $\hat{q}_j:=D_{jL}V_j$ induced by frequency deviation and voltage deviation, respectively. Moreover, we have the following assumption for $c_{pj}(p_j)$ and $c_{qj}(q_j)$.

Assumption 1: the cost functions $c_{pj}(p_j)$ and $c_{qj}(q_j)$ are strictly convex and twice continuously differentiable on $[\underline{p}_j,\bar{p}_j]$ and $[\underline{q}_j,\bar{q}_j]$, respectively.

In practice, cost functions refer to a specific target that considers the physical characteristics of household appliances, scheduling policies of utilities, and user comfort levels. Examples of cost functions satisfying our assumption can be found in [30] and [31].

B. Network Dynamics as Optimization Algorithm

The objective function of the dual problem of NOLC is represented as:

$$\sum_{j\in N}\Phi_j(v_j,\lambda_j)=\min_{\substack{\underline{p}_j\le p_j\le\bar{p}_j,\hat{p}_j,\\ \underline{q}_j\le q_j\le\bar{q}_j,\hat{q}_j}}\sum_{j\in N}\Bigg(c_{pj}(p_j)+c_{qj}(q_j)+\frac{1}{2D_j}\hat{p}_j^2+\frac{1}{2D_{jL}}\hat{q}_j^2-v_jp_j-v_j\hat{p}_j+v_jP_j^m+v_j\sum_{e\in\varepsilon}C_{je}P_e-\lambda_jq_j-\lambda_j\hat{q}_j+\lambda_jQ_j^m+\lambda_j\sum_{e\in\varepsilon}C_{je}Q_e\Bigg) \tag{20}$$

where the minimization $\Phi_j(v_j,\lambda_j)$ can be obtained as (21) with the optimality condition (22).

$$\Phi_j(v_j,\lambda_j)=c_{pj}(p_j(v_j))-v_jp_j(v_j)-\frac{1}{2}D_jv_j^2+v_jP_j^m-v_j\sum_{e\in\varepsilon}C_{je}P_e+c_{qj}(q_j(v_j))-\lambda_jq_j(v_j)-\frac{1}{2}D_{jL}\lambda_j^2+\lambda_jQ_j^m-\lambda_j\sum_{e\in\varepsilon}C_{je}Q_e \tag{21}$$

$$\begin{cases} \hat{p}_j:=D_jv_j \\ \hat{q}_j:=D_{jL}\lambda_j \\ p_j(v_j):=[(c_{pj}')^{-1}v_j]_{\underline{p}_j}^{\bar{p}_j} \\ q_j(\lambda_j):=[(c_{qj}')^{-1}\lambda_j]_{\underline{q}_j}^{\bar{q}_j} \end{cases} \tag{22}$$

According to the convex optimization theory, the Lagrange dual function is strictly concave. Therefore, the minimization of the primal problem can be transformed into the maximization of the dual problem.

$$\max_{v,\lambda}\Phi(v,\lambda):=\sum_{j\in N}\Phi_j(v_j,\lambda_j) \tag{23}$$

Based on the gradient descent algorithm iterating on each variable, the dynamics of v_j and λ_j follow the following rules.

$$\begin{cases} \dot{v}_j=\gamma_j\dfrac{\partial\Phi(v_j,\lambda_j)}{\partial v_j}=-\gamma_j\left(p_j(v_j)+D_jv_j-P_j^m-\sum_{e\in\varepsilon}C_{je}P_e\right) & \forall j\in G \\ \dot{\lambda}_j=\kappa_j\dfrac{\partial\Phi(v_j,\lambda_j)}{\partial\lambda_j}=-\kappa_j\left(q_j(\lambda_j)+D_{jL}\lambda_j-Q_j^m-\sum_{e\in\varepsilon}C_{je}Q_e\right) & \forall j\in L \end{cases} \tag{24}$$

Among that, $\gamma_j>0$ and $\kappa_j>0$ are step sizes, which can be defined as:

$$\begin{cases} \gamma_j=\dfrac{1}{H_j} \\ \kappa_j=\dfrac{1}{K_j} \end{cases} \tag{25}$$

By replacing v_j and λ_j with ω_j and V_j, respectively, where ω_j and V_j are the design variables of the dual problem, (24) would be the same as the network dynamics shown in (14) and (15). In other words, the network dynamics can be regarded as distributed algorithms for a dual problem under optimality conditions in (22).

$$\dot{\omega}_j=-\frac{1}{H_j}\left(p_j(\omega_j)+D_j\omega_j-P_j^m+\sum_{e\in\varepsilon}C_{je}P_e\right)\quad\forall j\in G \tag{26}$$

$$\dot{V}_j=-\frac{1}{K_j}\left(q_j(V_j)+D_{jL}V_j-Q_j^m+\sum_{e\in\varepsilon}C_{je}Q_e\right)\quad\forall j\in L \tag{27}$$

$$\hat{p}_j:=D_j\omega_j\quad\forall j\in N \tag{28}$$

$$\hat{q}_j:=D_{jL}V_j\quad\forall j\in N \tag{29}$$

$$p_j(\omega_j):=[(c_{pj}')^{-1}\omega_j]_{\underline{p}_j}^{\bar{p}_j}\quad\forall j\in N \tag{30}$$

$$q_j(V_j):=[(c_{qj}')^{-1}V_j]_{\underline{q}_j}^{\bar{q}_j}\quad\forall j\in N \tag{31}$$

The dynamics (26) - (29) are performed automatically by the system, whereas the active power consumption control in (30) and reactive power consumption control in (31) must be applied to each controllable load. Therefore, the analyses develop a fundamental method to guide the design of the local load control, and we refer to this as the NOLC. Under such a control, the controllable loads can share the overall power imbalance, and the disturbance will not severely affect any single bus.

Regardless of the initial conditions, (26) - (31) establish a trajectory $(\boldsymbol{p}(t),\hat{\boldsymbol{p}}(t),\boldsymbol{q}(t),\hat{\boldsymbol{q}}(t),\boldsymbol{\omega}(t),\boldsymbol{V}(t))$ that converges to the optimal point $(\boldsymbol{p}^*,\hat{\boldsymbol{p}}^*,\boldsymbol{q}^*,\hat{\boldsymbol{q}}^*,\boldsymbol{\omega}^*,\boldsymbol{V}^*)$ with $t\to+\infty$. $[\boldsymbol{p}^*,\hat{\boldsymbol{p}}^*,\boldsymbol{q}^*,\hat{\boldsymbol{q}}^*]$ is a unique vector of the optimal load control for the primal problem, and $[\boldsymbol{\omega}^*,\boldsymbol{V}^*]$ is a unique vector of the optimal frequency and voltage deviations for the dual problem. The proof is as follows.

Proof: following the Lyapunov stability theory, a Lyapunov function, as constructed below, is analyzed. Let $\boldsymbol{x}:=[\boldsymbol{\omega},\boldsymbol{V}]^{\mathrm{T}}$, and we can obtain:

$$U(\boldsymbol{x})=\frac{1}{2}(\boldsymbol{x}-\boldsymbol{x}^*)^{\mathrm{T}}\begin{bmatrix}\gamma^{-1} & 0\\ 0 & \kappa^{-1}\end{bmatrix}(\boldsymbol{x}-\boldsymbol{x}^*) \tag{32}$$

$$U(\boldsymbol{\omega},\boldsymbol{V})=\frac{1}{2}(\boldsymbol{\omega}_G-\boldsymbol{\omega}_G^*)^{\mathrm{T}}\gamma_G^{-1}(\boldsymbol{\omega}_G-\boldsymbol{\omega}_G^*)+\frac{1}{2}(\boldsymbol{V}_L-\boldsymbol{V}_L^*)^{\mathrm{T}}\kappa_L^{-1}(\boldsymbol{V}_L-\boldsymbol{V}_L^*) \tag{33}$$

where $\boldsymbol{\omega}_G$ and $\boldsymbol{V}_L$ are the frequency deviations on generator buses and voltage deviations on load buses, respectively, and $\boldsymbol{\omega}_G^*$ and $\boldsymbol{V}_L^*$ denote their optimal values.

Distinctly, $U(\boldsymbol{\omega},\boldsymbol{V})\geq 0$ for all $\boldsymbol{x}$ with equality if and only if $\boldsymbol{\omega}=\boldsymbol{\omega}_G^*$ and $\boldsymbol{V}=\boldsymbol{V}_L^*$. $\dot{U}(\boldsymbol{\omega},\boldsymbol{V})$ expresses the derivative of U over time along the trajectory $(\boldsymbol{\omega}(t),\boldsymbol{V}(t))$. If $\dot{U}(\boldsymbol{\omega},\boldsymbol{V})\leq 0$, for all $\boldsymbol{x}$, $(\boldsymbol{\omega}(t),\boldsymbol{V}(t))$ will be converged to $(\boldsymbol{\omega}^*,\boldsymbol{V}^*)$ finally with

$$\dot{\boldsymbol{\omega}}_G=\left[\gamma_G\frac{\partial\Phi(\boldsymbol{\omega}_G,\boldsymbol{V}_L)}{\partial\boldsymbol{\omega}_G}\right]^{\mathrm{T}} \tag{34}$$

$$\dot{\boldsymbol{V}}_L=\left[\kappa_L\frac{\partial\Phi(\boldsymbol{\omega}_G,\boldsymbol{V}_L)}{\partial\boldsymbol{V}_L}\right]^{\mathrm{T}} \tag{35}$$

The derivative $\dot{U}(\boldsymbol{\omega},\boldsymbol{V})$ of the Lyapunov function $U(\boldsymbol{x})$ along any trajectory $(\boldsymbol{\omega}(t),\boldsymbol{V}(t))$ can be easily converted from ① to ② in (36).

$$\begin{aligned}\dot{U}(\boldsymbol{\omega},\boldsymbol{V})&=(\boldsymbol{\omega}_G-\boldsymbol{\omega}_G^*)^{\mathrm{T}}\gamma_G^{-1}\dot{\boldsymbol{\omega}}_G+(\boldsymbol{V}_L-\boldsymbol{V}_L^*)^{\mathrm{T}}\kappa_L^{-1}\dot{\boldsymbol{V}}_L\overset{①}{=}\\&\frac{\partial\Phi(\boldsymbol{\omega}_G,\boldsymbol{V}_L)}{\partial\boldsymbol{\omega}_G}(\boldsymbol{\omega}_G-\boldsymbol{\omega}_G^*)+\frac{\partial\Phi(\boldsymbol{\omega}_G,\boldsymbol{V}_L)}{\partial\boldsymbol{V}_L}(\boldsymbol{V}_L-\boldsymbol{V}_L^*)\overset{②}{\leq}\\&\Phi(\omega_G,V_L)-\Phi(\boldsymbol{\omega}_G^*,\boldsymbol{V}_L)+\Phi(\boldsymbol{\omega}_G,\boldsymbol{V}_L)-\Phi(\boldsymbol{\omega}_G,\boldsymbol{V}_L^*)\overset{③}{\leq}0\end{aligned} \tag{36}$$

Due to the strong concavity of the objective function in dual problem, the inequality ② holds since Lagrange's mean value theorem. Moreover, $\Phi(\boldsymbol{\omega}_G^*,\boldsymbol{V}_L)$ is larger than $\Phi(\boldsymbol{\omega}_G,\boldsymbol{V}_L)$, and $\Phi(\boldsymbol{\omega}_G,\boldsymbol{V}_L^*)$ is larger than $\Phi(\boldsymbol{\omega}_G,\boldsymbol{V}_L)$, satisfying ③. Therefore, for all $\boldsymbol{x}:=[\boldsymbol{\omega},\boldsymbol{V}]^{\mathrm{T}}$, $\dot{U}(\boldsymbol{\omega},\boldsymbol{V})\leq 0$ is proved.

C. Load Controller Designing for Specific Disutility Function

Once the cost functions satisfy the assumptions of strict convexity and twice continuous differentiability in the feasible region, NOLC can be implemented successfully at the demand side. Moreover, the power consumption controls for smart loads vary depending on the type of cost function. A specified control signal can be obtained for a given cost function.

If the cost functions are the quadratic forms of $c_{pj}(p_j)=p_j^2/(2\alpha)$ and $c_{qj}(q_j)=q_j^2/(2\beta)$ (α and β are both positive numbers), the active control signal of the controllable loads for this simple cost function is $p_j(\omega_j):=[(c'_{pj})^{-1}\omega_j]_{\underline{p}_j}^{\bar{p}_j}=\alpha\omega_j$, and the reactive control signal is $q_j(V_j):=[(c'_{qj})^{-1}V_j]_{\underline{q}_j}^{\bar{q}_j}=\beta V_j$. Under this circumstance, Fig. 1 shows the block diagram of NOLC under specific disutility function built in Simulink, where f is the system frequency; f^* is the frequency reference; V is the voltage; V^* is the voltage reference; and P_0 and Q_0 are the original active and reactive load power, respectively.

IV. Small-signal Analysis

In this section, the effect of NOLC on the system small-signal stability is investigated.

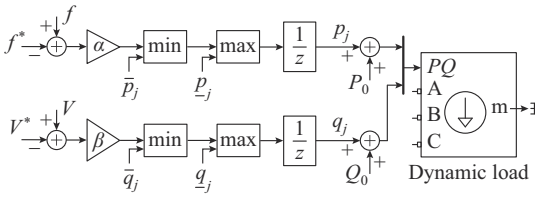

Fig. 1. NOLC under specific disutility function.

As an illustration, the OLC for the cost function discussed in the previous section is applied to the standard IEEE 33-bus power system. The detailed information regarding the test system is presented in [32]. The reference value of the nodal voltage is 12.66 kV, and the total load of the system is (3715+j2300)kVA.

It consists of 1 generator bus, 32 load buses, and 32 branches. Node 1 is selected as the generator bus; nodes 3, 18, 25, and 28 are selected as the disturbance buses (renewable sources or loads can cause power disturbances in a real situation); and nodes 4, 7, 15, 21, 23, and 32 are selected as controllable buses to accomplish the NOLC. As shown in Table I, the sum of the controllable active loads is set to be 9 kW (0.24% of the total active loads), and the sum of the controllable reactive loads is set to be 5.52 kvar (0.24% of the total reactive loads).

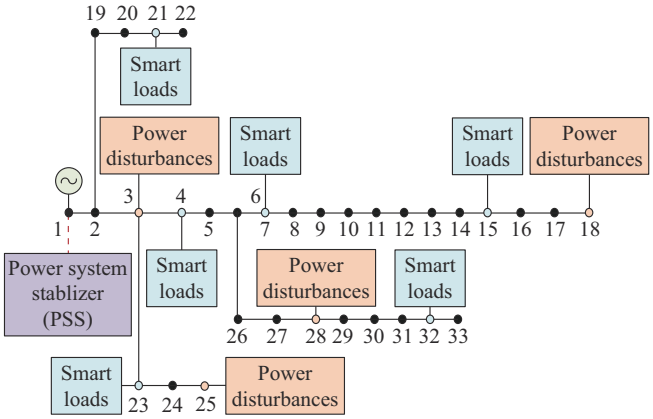

Fig. 2. Topological structure of IEEE 33-bus power system.

TABLE I
Load Bounds of Buses

Bus No.	Norm		Controllable		Non-controllable	
	P (kW)	Q (kvar)	P (kW)	Q (kvar)	P (kW)	Q (kvar)
4	120	80	1.40	1.165	118.60	78.835
7	200	100	2.35	1.450	197.65	98.550
15	60	10	0.70	0.145	59.30	9.855
21	90	40	1.05	0.580	88.95	39.420
23	90	50	1.05	0.730	88.95	49.270
32	210	100	2.45	1.450	207.55	98.550
Sum	770	380	9.00	5.520	761.00	374.480

According to the network model built in Section II, the state variables and operation variables are selected as $[\boldsymbol{\theta},\boldsymbol{\omega}_G,\boldsymbol{V}_L]$ and $[\boldsymbol{\omega}_L,\boldsymbol{p},\boldsymbol{q},\boldsymbol{P}_{ij},\boldsymbol{Q}_{ij}]$, respectively. Therefore, the

state-space equations of the power system are represented as:

$$\left[\frac{\mathrm{d}\boldsymbol{\theta}}{\mathrm{d}t} \quad \frac{\mathrm{d}\boldsymbol{\omega}_G}{\mathrm{d}t} \quad \frac{\mathrm{d}\boldsymbol{V}_L}{\mathrm{d}t} \quad \mathbf{0}\right]^{\mathrm{T}} = \begin{bmatrix}\tilde{\boldsymbol{A}} & \tilde{\boldsymbol{B}} \\ \tilde{\boldsymbol{C}} & \tilde{\boldsymbol{D}}\end{bmatrix} \cdot [\boldsymbol{\theta} \quad \boldsymbol{\omega}_G \quad \boldsymbol{V}_L \quad \boldsymbol{\omega}_L \quad \boldsymbol{p} \quad \boldsymbol{q} \quad \boldsymbol{P}_{ij} \quad \boldsymbol{Q}_{ij}]^{\mathrm{T}} \tag{37}$$

where $\tilde{\boldsymbol{A}}$, $\tilde{\boldsymbol{B}}$, $\tilde{\boldsymbol{C}}$, and $\tilde{\boldsymbol{D}}$ are the corresponding coefficient matrices.

The system state matrix $\boldsymbol{A}$ can be defined as:

$$\boldsymbol{A} = \tilde{\boldsymbol{A}} - \tilde{\boldsymbol{B}}\tilde{\boldsymbol{D}}^{-1}\tilde{\boldsymbol{C}} \tag{38}$$

All the eigenvalues of the system state matrix $\boldsymbol{A}$ with $\alpha = \alpha_0 = 50$ p.u. and $\beta = \beta_0 = 20$ p.u. possess a negative real part; therefore, the small-signal stability is verified.

To investigate the influence of the parameter variations on the load controllers for system stability, more details regarding the experimental settings are presented in Table II.

TABLE II
EXPERIMENTAL SETTINGS

Cost function	Control signal	Parameter variation
$\frac{p_j^2}{2\alpha_0} + \frac{q_j^2}{2\beta_0}$	$p_j(\omega_j) = \alpha\omega_j$, $q_j(V_j) = \beta V_j$	$\alpha \in [0.98\alpha_0, 1.02\alpha_0]$, $\beta \in [0.98\beta_0, 1.02\beta_0]$

The locus distribution of the dominant eigenvalues (the absolute values of the real parts of the other eigenvalues are at least five times those near the imaginary axis) is shown in Fig. 3 under the condition of an increasing trend of α and β simultaneously. Moreover, α is from 49 p.u. to 51 p.u., and β is from 19.6 p.u. to 20.4 p.u..

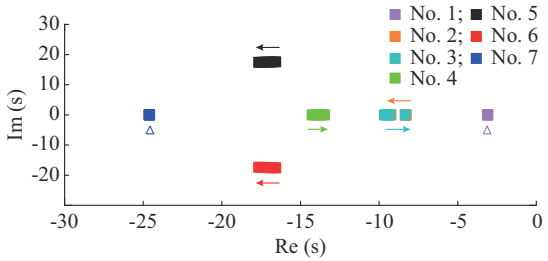

Fig. 3. Locus distribution of dominant eigenvalues.

According to Fig. 3, No. 1 and No. 7 poles almost remain the same, and the positions of other dominant eigenvalues do not change significantly. Therefore, the real parts of eigenvalues are still all negative with ±2% variations of parameters α and β, and the system stays stable. Hence, the inevitable parameter variation within a reasonable range is acceptable to the load controller.

V. SIMULATION RESULTS

The test system is shown in Fig. 2. The smart loads consist of controllable and non-controllable parts represented by three-phase parallel RLC loads and three-phase three-wire dynamic loads in Simulink, respectively. The controllable loads are set with identical $\alpha = 50$ p.u. and $\beta = 20$ p.u. in the test system. According to a conservative estimate of the rate of load control in an existing test bed, the control time of the dynamic loads is 250 ms [13].

A. NOLC v.s. Traditional OLC v.s. LVC

To observe the difference in the frequency/voltage dynamic response over the load participation in the primary control among the proposed NOLC, traditional OLC [21], and LVC [25], conclusions are drawn based on the simulation results. Figure 4(a) and (b) shows the frequency and voltage dynamics on bus 4 after the load disturbance, respectively.

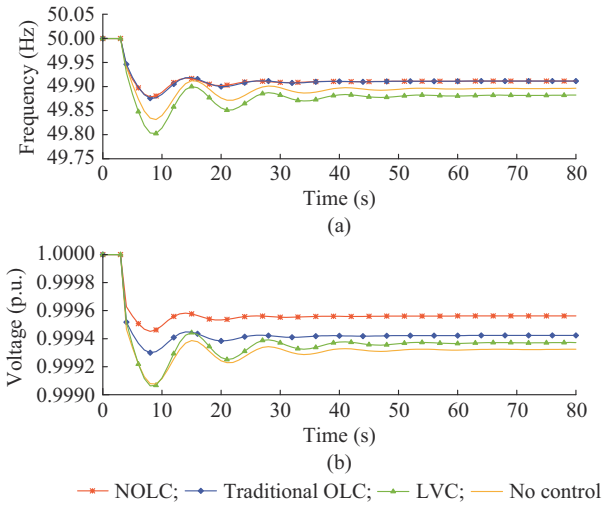

Fig. 4. Frequency and voltage on bus 4 after load disturbance. (a) Frequency. (b) Voltage.

As shown in Fig. 4, the LVC provides voltage support compared to the case without control; however, it negatively affects the frequency stability. Unlike the LVC applied on the load side, the NOLC and traditional OLC perform better in terms of both transient and steady-frequency performances.

Although the NOLC has the benefits similar to the traditional OLC in primary frequency control, the voltage nadir is suppressed by 21.4%, and the steady-state error is improved by approximately 24.2%. The traditional OLC ignores the load participation ability in voltage regulation through a reasonable reactive control. In summary, the NOLC enables the smart loads on the user side to contribute to the primary control of both frequency and voltage.

Moreover, the NOLC considers the aggregate disutility of load participation in primary regulation. The cost function trajectory of the NOLC over time, which is calculated according to (19) using the simulation results, is shown in Fig. 5. Finally, the cost converges to a minimum value for a specified load disturbance.

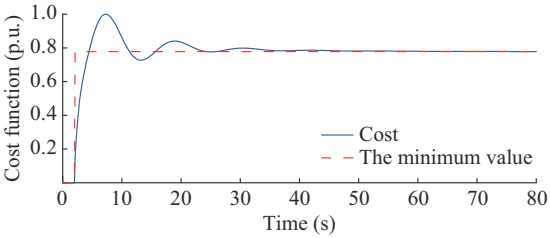

Fig. 5. Cost function trajectory of NOLC.

B. Coordination with Other Devices

In this subsection, we discuss the coordination between the NOLC and other devices enabled in the system to cope with power disturbances.

1) Scenario 1: Coordination with TG

The primary control capability of power systems is closely related to the adjustment coefficients of traditional generators (TGs). The smaller the adjustment coefficient σ is, the greater load TG carries when the same frequency drops. In Fig. 6(a) and (b), with the participation of NOLC under a small σ, when the frequency and voltage nadirs increase, the settling time becomes shorter. The frequency fluctuations and voltage drops are mitigated by controlling the power consumption of the controllable loads.

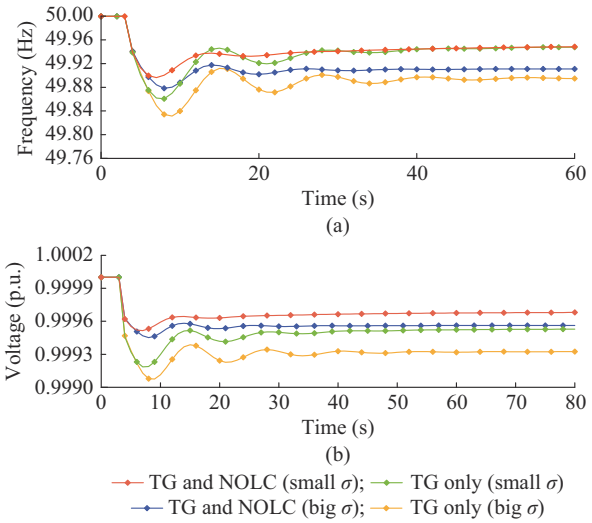

Fig. 6. Frequency and voltage on bus 4 with coordination of TG and NOLC. (a) Frequency. (b) Voltage.

However, the adjustment coefficient cannot be too low for the stable operation of the generator governor. Therefore, the NOLC is required when the primary control ability of the TG is relatively insufficient. In Fig. 6(a) and (b), with the participation of the NOLC under a large σ, the transient response and steady state of both the system frequency and voltage are improved.

It has been found that applying the NOLC to the system leads to a higher frequency/voltage nadir (i. e., a smaller overshoot), a higher new steady-state frequency/voltage, and a shorter settling time.

2) Scenario 2: Coordination with PSS

We present the simulation results for a PSS, which is a widely-used generation-side stabilizing mechanism.

Compared with the above cases, the fluctuations in both frequency and voltage are intuitively suppressed due to the function of the PSS. It is clear from Fig. 7(a) and (b) that deeper frequency and voltage support are provided when the NOLC works with PSS.

From the simulation results in Sections V-A and V-B, whether the PSS is enabled or not, applying the proposed NOLC on the user side improves the frequency and voltage dynamics.

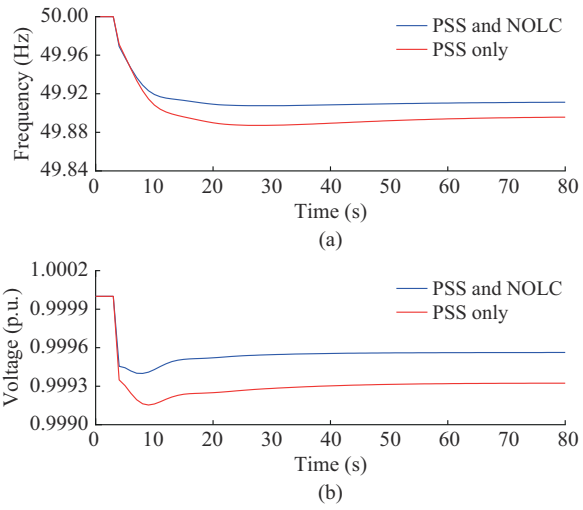

Fig. 7. Frequency and voltage on bus 4 with coordination of PSS. (a) Frequency. (b) Voltage.

C. NOLC Performance Against Total Size of Controllable Loads

In this subsection, the NOLC performance is plotted against the total size of the controllable loads. Figure 8 shows that the lowest and steady-state frequencies increase with the increasing load participation in the primary control. The labels on the x-axis represent the number of controllable loads (among buses 4, 7, 15, 21, 23, 32) put into use.

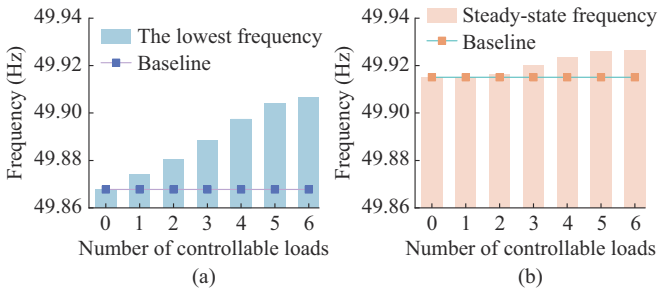

Fig. 8. Effects on frequency of NOLC with increasing number of controllable loads. (a) The lowest frequency. (b) Steady-state frequency.

A similar trend can also be observed for the voltage, as shown in Fig. 9. Both the lowest and steady-state voltages exhibit a performance improvement as the number of the controllable loads increases.

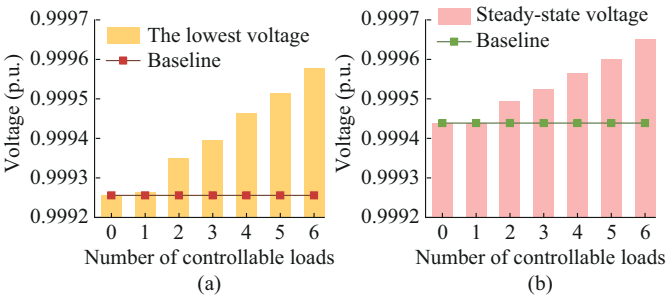

Fig. 9. Effects on voltage of NOLC with increasing number of controllable loads. (a) The lowest voltage. (b) Steady-state voltage.

The rapid growth of smart loads has become a developmental trend in modern power systems and provides a good basis for the NOLC applications.

D. NOLC Performance in Multi-machine Networks

In this subsection, we investigate the performance of the NOLC in terms of both the transient response and the steady states of system frequency and voltage in a multi-machine network. A single-line diagram of the New England 39-bus power system is shown in Fig. 10. As shown in Fig. 10, there are 10 generators and 19 load buses. Nodes 18 and 27 are selected as disturbance buses. Nodes 4, 7, 15, 21, 23, and 28 are selected as controllable buses to accomplish the NOLC, and the controllable loads that are available to participate in the primary control account for 20% of their total amount.

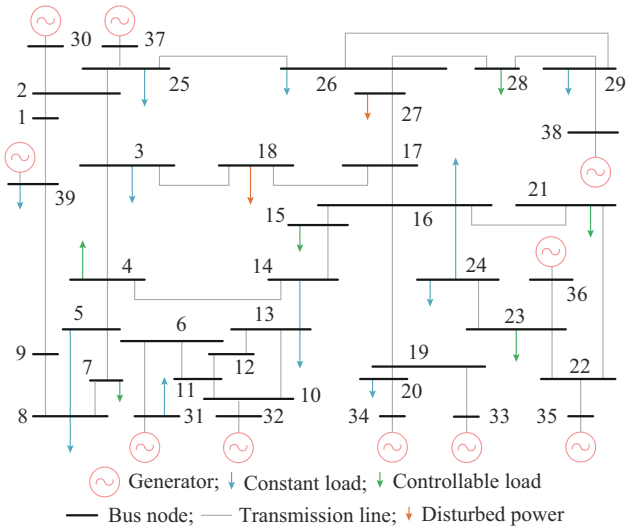

Fig. 10. Single-line diagram of New England 39-bus power system.

Figures 11 and 12 show the system frequency and bus voltage dynamics using NOLC, respectively. As shown in Fig. 11, adding NOLC to the power system provides remarkable benefits in the primary frequency control with respect to both nadir and steady-state errors.

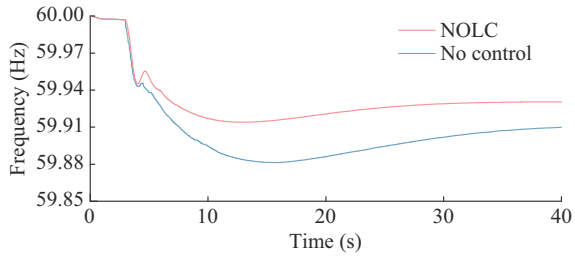

Fig. 11. Frequency dynamics of New England 39-bus power system.

Moreover, as shown in Fig. 12, the voltage dynamics on the load buses are also improved. The voltage nadirs are suppressed and the steady-state errors are decreased using the NOLC.

The simulation results indicate the effectiveness of applying the NOLC to a multi-machine power system.

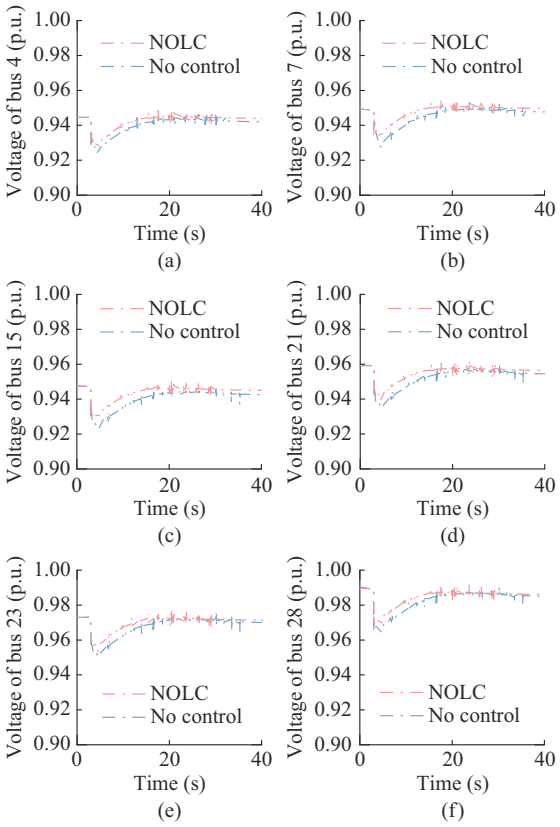

Fig. 12. Voltage dynamics of New England 39-bus power system. (a) Bus 4. (b) Bus 7. (c) Bus 15. (d) Bus 21. (e) Bus 23. (f) Bus 28.

VI. Conclusion

We propose a method to design load control by considering network dynamics as optimization algorithms to enable smart loads on the demand side to contribute to the primary frequency and voltage control.

Compared with existing methods, the proposed NOLC ensures the aggregate disutility is minimized while rebalancing the power and improving the transient performances of both frequency and voltage. Since the participation of controllable loads is completely distributed, their power consumption can be determined individually according to local measurements of the frequency/voltage deviation. The NOLC generates a faster response and better steady-state performance with the coordination of other devices enabled in power systems, such as TGs and PSS, and the power imbalance is compensated on time. Moreover, the effectiveness of the NOLC in a multi-machine power system is verified.

Although the simulation results reveal that the total number of controllable loads influences the regulation performance of NOLC and that the practical implementation of this technology relies on several power meters, these challenges can be solved gradually with the rapid development of smart grids. Our future scope includes the further development of new idea-network dynamics as optimization algorithms for the distributed control and optimization of modern power systems.

APPENDIX A

The branch active power flow P_{ij} from i to j is expressed as:

$$P_{ij}=-V_iV_j(g_{ij}\cos\theta_{ij}+b_{ij}\sin\theta_{ij})+g_{ij}V_i^2\approx V_iV_jB_{ij}\sin\theta_{ij} \quad \text{(A1)}$$

where $B_{ij}=-b_{ij}=-(-1/x_{ij})=1/x_{ij}$.

In the case of a small disturbance, the deviation values of the variables are approximately the same as the normal values; so, the equation can be linearized as:

$$\Delta P_{ij}=\frac{\partial\Delta P_{ij}}{\partial\Delta V_i}\Delta V_i+\frac{\partial\Delta P_{ij}}{\partial\Delta V_j}\Delta V_j+\frac{\partial\Delta P_{ij}}{\partial(\Delta\theta_i-\Delta\theta_j)}(\Delta\theta_i-\Delta\theta_j)\approx V_j^0B_{ij}\sin(\theta_i^0-\theta_j^0)\Delta V_i+V_i^0B_{ij}\sin(\theta_i^0-\theta_j^0)\Delta V_j+V_i^0V_j^0B_{ij}\cos(\theta_i^0-\theta_j^0)(\Delta\theta_i-\Delta\theta_j) \quad \text{(A2)}$$

Thus, $\Delta P_{ij}=B'_{ij}\Delta V_i+B''_{ij}\Delta V_j+B'''_{ij}(\Delta\theta_i-\Delta\theta_j)$ with $B'_{ij}=V_j^0\sin(\theta_i^0-\theta_j^0)/x_{ij}$, $B''_{ij}=V_i^0\sin(\theta_i^0-\theta_j^0)/x_{ij}$, and $B'''_{ij}=V_i^0V_j^0\cos(\theta_i^0-\theta_j^0)/x_{ij}$.

Similarly, the branch reactive power from i to j is:

$$Q_{ij}=-V_iV_j(g_{ij}\sin\theta_{ij}-b_{ij}\cos\theta_{ij})-b_{ij}V_i^2\approx B_{ij}V_i^2-V_iV_jB_{ij}\cos\theta_{ij} \quad \text{(A3)}$$

Additionally, the linearized function is:

$$\Delta Q_{ij}\approx 2B_{ij}V_i^0\Delta V_i-V_j^0B_{ij}\cos(\theta_i^0-\theta_j^0)\Delta V_i-V_i^0B_{ij}\cos(\theta_i^0-\theta_j^0)\Delta V_j+V_i^0V_j^0B_{ij}\sin(\theta_i^0-\theta_j^0)(\Delta\theta_i-\Delta\theta_j) \quad \text{(A4)}$$

Hence, $\Delta Q_{ij}=T'_{ij}\Delta V_i+T''_{ij}\Delta V_j+T'''_{ij}(\Delta\theta_i-\Delta\theta_j)$ with $T'_{ij}=2V_i^0/x_{ij}-V_j^0\cos(\theta_i^0-\theta_j^0)/x_{ij}$, $T''_{ij}=-V_i^0\cos(\theta_i^0-\theta_j^0)/x_{ij}$ and $T'''_{ij}=V_i^0V_j^0\sin(\theta_i^0-\theta_j^0)/x_{ij}$.

REFERENCES

[1] M. W. Altaf, M. T. Arif, S. Saha *et al*., "Renewable energy integration challenge on power system protection and its mitigation for reliable operation," in *Proceedings of Industrial Electronics Conference (IECON)*, Singapore, Oct. 2020, pp. 1917-1922.

[2] I. Dusparic, A. Taylor, A. Marinescu *et al.*, "Maximizing renewable energy use with decentralized residential demand response," in *Proceedings of 2015 IEEE First International Smart Cities Conference (ISC2)*, Guadalajara, Mexico, Dec. 2015, pp. 1-6.

[3] M. Bayat, K. Sheshyekani, and A. Rezazadeh, "A unified framework for participation of responsive end-user devices in voltage and frequency control of the smart grid," *IEEE Transactions on Power Systems*, vol. 30, no. 3, pp. 1369-1379, May 2015.

[4] H. Rezk, M. A. Mohamed, A. Diab *et al.*, "Load frequency control of multi-interconnected renewable energy plants using multi-verse optimizer," *Computer Systems Science and Engineering*, vol. 37, no.2, pp. 219-231, Mar. 2021.

[5] G. Tan, C. Xu, F. Wu *et al.*, "Research on primary frequency regulation of wind turbine based on new nonlinear droop control," in *Proceedings of 2020 4th International Conference on HVDC (HVDC)*, Xi'an, China, Nov. 2020, pp. 170-174.

[6] H. Xin, L. Zhang, Z. Wang *et al.*, "Control of island AC microgrids using a fully distributed approach," *IEEE Transactions on Smart Grid*, vol. 6, no. 2, pp. 943-945, Mar. 2015.

[7] Y. Kinjyo, M. Miyagi, T. Senjyu *et al.*, "Decentralized controllable loads control in small power system," in *Proceedings of Renewable Energy Research and Applications (ICRERA)*, Nagasaki, Japan, Nov. 2012, pp. 1-6.

[8] M. Tokudome, K. Tanaka, T. Senjyu *et al.*, "Frequency and voltage control of small power systems by decentralized controllable loads," in *Proceedings of the International Conference on Power Electronics and Drive Systems(PEDS)*, Taipei, China, Nov. 2009, pp. 666-671.

[9] D. S. Callaway and I. A. Hiskens, "Achieving controllability of electric loads," *Proceedings of the IEEE*, vol. 99, no. 1, pp.184-199, Jan. 2011.

[10] A. S. A. Awad, D. Turcotte, and T. H. M. El-Fouly, "Impact assessment and mitigation techniques for high penetration levels of renewable energy sources in distribution networks: voltage-control perspective," *Journal of Modern Power Systems and Clean Energy*, vol. 10, no. 2, pp. 450-458, Mar. 2022.

[11] Y. Weng, R. Rajagopal, and B. Zhang, "A geometric analysis of power system loadability regions," *IEEE Transactions on Smart Grid*, vol. 11, no. 4, pp. 3580-3592, Jul. 2020.

[12] F. C. Schweppe, R. D. Tabors, J. L. Kirtley *et al*., "Homeostatic utility control," *IEEE Transactions on Power Apparatus and Systems*, vol. PAS-99, no. 3, pp. 1151-1163, May 1980.

[13] P. J. Douglass, R. Garcia-Valle, P. Nyeng *et al.*, "Smart demand for frequency regulation: experimental results," *IEEE Transactions on Smart Grid*, vol. 4, no. 3, pp. 1713-1720, Jul. 2013.

[14] Y. Kinjyo, M. D. Palmer, A. Yona *et al.*, "Autonomous power system control by decentralized controllable loads," in *Proceedings of the International Conference on Power Electronics and Drive Systems (PEDS)*, Kitakyushu, Japan, Nov. 2013, pp. 881-886.

[15] I. Jendoubi, K. Sheshyekani, and H. Dagdougui, "Aggregation and optimal management of TCLs for frequency and voltage control of a microgrid," *IEEE Transactions on Power Delivery*, vol. 36, no. 4, pp. 2085-2096, Aug. 2021.

[16] A. Takahashi, N. Matsumoto, J. Imai *et al.*, "A voltage control method using EVs in the power distribution system including a mass of PVs," in *Proceedings of 2017 IEEE 12th International Conference on Power Electronics and Drive Systems (PEDS)*, Honolulu, USA, Dec. 2017, pp. 507-510.

[17] S. H. Low, "Convex relaxation of optimal power flow – Part I: formulations and equivalence," *IEEE Transactions on Control of Network Systems*, vol. 1, no. 1, pp. 15-27, Mar. 2014.

[18] S. H. Low, "Convex relaxation of optimal power flow – Part II: exactness," *IEEE Transactions on Control of Network Systems*, vol. 1, no. 2, pp. 177-189, Jun. 2014.

[19] Q. Peng and S. H. Low, "Distributed optimal power flow algorithm for radial networks, I: balanced single phase case," *IEEE Transactions on Smart Grid*, vol. 9, no. 1, pp. 111-121, Jan. 2018.

[20] C. Zhao, U. Topcu, and S. Low, "Swing dynamics as primal-dual algorithm for optimal load control," in *Proceedings of 2012 IEEE 3rd International Conference on Smart Grid Communications*, Tainan, China, Nov. 2012, pp. 570-575.

[21] C. Zhao, U. Topcu, N. Li *et al.*, "Design and stability of load-side primary frequency control in power systems," *IEEE Transactions on Automatic Control*, vol. 59, no. 5, pp. 1177-1189, May 2014.

[22] I. Kamwa and A. Delavari, "Simulation-based investigation of optimal demand-side primary frequency regulation," in *Proceedings of Canadian Conference on Electrical and Computer Engineering (CCECE)*, Vancouver, Canada, Oct. 2016, pp. 1-6.

[23] A. Delavari and I. Kamwa, "Improved optimal decentralized load modulation for power system primary frequency regulation," *IEEE Transactions on Power Systems*, vol. 33, no. 1, pp. 1013-1025, Jan. 2018.

[24] M. Farivar, X. Zho, and L. Che, "Local voltage control in distribution systems: an incremental control algorithm," in *Proceedings of 2015 IEEE International Conference on Smart Grid Communications (SmartGridComm)*, Miami, USA, Nov. 2015, pp. 732-737.

[25] M. Ghazzali, M. Haloua, and F. Giri, "Fixed-time distributed voltage and reactive power compensation of islanded microgrids using sliding-mode and multi-agent consensus design," *Journal of Modern Power Systems and Clean Energy*, vol. 10, no. 1, pp. 232-240, Jan. 2022.

[26] Y. Wang, D. Qi, and J. Zhang, "Multi-objective optimization for voltage and frequency control of smart grids based on controllable loads," *Global Energy Interconnection*, vol. 4, no. 2, pp. 136-144, Apr. 2021.

[27] S. Magnússon, G. Qu, and N. Li, "Distributed optimal voltage control with asynchronous and delayed communication," *IEEE Transactions on Smart Grid*, vol. 11, no. 4, pp. 3469-3482, Jul. 2020.

[28] M. D. Ilić, L. Xie, U. A. Khan *et al.*, "Modeling of future cyberphysical energy systems for distributed sensing and control," *IEEE Transactions on Systems, Man, & Cybernetics Part A: Systems & Humans*, vol. 40, no. 4, pp. 825-838, Jul. 2010.

[29] K. T. Vu and C. C. Liu, "Shrinking stability regions and voltage collapse in power systems," *IEEE Transactions on Circuits and Systems I: Fundamental Theory and Applications*, vol. 39, no. 4, pp. 271-289, Apr. 1992.

[30] B. Ramanathan and V. Vittal, "A framework for evaluation of advanced direct load control with minimum disruption," *IEEE Transactions on Power Systems*, vol. 23, no. 4, pp. 1681-1688, Nov. 2008.

[31] K. Ma, Z. Jiao, and J. Yang, "A hierarchical scheduling strategy of thermostatically controlled loads in smart grid," in *Proceedings of*

IEEE International Conference on Control and Automation (ICCA), Singapore, Oct. 2020, pp. 1278-1283.

[32] M. A. Kashem, V. Ganapathy, G. B. Jasmon *et al.*, "A novel method for loss minimization in distribution networks," in *Proceeding of Electric Utility Deregulation and Restructuring and Power Technologies*, London, UK, Apr. 2000, pp. 251-256.

Yaxin Wang received her B.E. degree in electrical engineering from Zhengzhou University, Zhengzhou, China, in 2019. She is currently pursuing her Ph.D. degree in electrical engineering from Zhejiang University, Hangzhou, China. Her research interests include voltage and frequency optimization control in smart grids, and game theory-based distributed optimization with applications to power systems.

Donglian Qi received her Ph.D. degree in control theory and control engineering from Zhejiang University, Hangzhou, China, in March 2002. Since then, she has been with the College of Electrical Engineering, Zhejiang University, where she is currently a Professor. She is an Editor for the Clean Energy, the IET Energy Conversion and Economics, and the Journal of Robotics, Networking and Artificial Life. Her current research interests include the basic theory and application of cyber physical power system (CPPS), digital image processing, artificial intelligence, and electric operation and maintenance robots.

Jianliang Zhang received his Ph.D. degree in control theory and control engineering from Zhejiang University, Hangzhou, China, in June 2014. Since then, he has been working with College of Electrical Engineering, Zhejiang University. He was a Visiting Scholar at Hong Kong Polytechnic University (PolyU), Hong Kong, China, from 2016 to 2017. His current research interests include distributed optimization, with applications to energy/power systems, and cyber-physical security with applications in smart grids.

Jingcheng Mei received his B.E. degree in electrical engineering from Wuhan University of Technology, Wuhan, China, in 2012, and his M.S. degree in electrical engineering from Wuhan University, Wuhan, China, in 2014. He is currently pursuing his Ph.D. degree at the College of Electrical Engineering, Zhejiang University, Hangzhou, China. His current research interests include machine-learning, combinatorial optimization and uncertainty optimization, with applications to energy/power systems.